Electro-Oxidation of Titanium Carbide Nanoparticles in Aqueous Acid Creates TiC@TiO$_2$ Core-Shell Structures

Pranati Nayak,[a] Ruo-Chen Xie,[a] Robert G. Palgrave,[b] and Richard G. Compton*[a]

Titanium carbide (TiC) is an attractive support material used in electro-catalysis and sensing. We report the electrochemistry of TiC nanoparticles (NPs, 35–50 nm in diameter) in different electrolytes in the pH range of 0 to 8. The TiC NPs undergo irreversible oxidation in acidic, basic, and neutral media, attributed to the partial conversion into titanium dioxide (TiO$_2$) with the amount of oxidation highly dependent on the pH of the solution. In H$_2$SO$_4$ (pH 0), multiple voltammetric scans revealed the conversion to be partial but repeated scans allowed a conversion approaching 100% to be obtained with 20 scans generating a ca 60% level of oxidation. The process is inferred to lead to the formation of TiC@TiO$_2$ core-shell nano-particles (∼12.5 nm core radius and ∼5 nm shell width for a 60% conversion) and this value sharply decreases with an increase of pH. Independent measurements were conducted at a single NP level (via nano-impact experiments) to confirm the oxidation of the NPs, showing consistent agreement with the bulk measurements.

1. Introduction

Transition metal carbides (TMCs) are earth-abundant ceramics having metallic electrical conductivity, high specific surface area, and melting points, often used as support materials for single-atom catalysts (SACs), nanoparticle catalysts, and electro-chemical sensing.[1–3] Contemporary research on SACs feature atomically dispersed precious metals (< 1 wt%) over TMC supports (e.g. TiC, WC, TiN, Mo$_2$C, etc.), where electronically bound atomic metals to promote catalysis with claims of "100% metal utilization efficiency".[4,5] A similar application occurs in nanoparticle catalysis, where catalyst NPs are dispersed over TMC supports preventing agglomeration and enabling max-imum utilization of nanoparticles.[6] Similarly, in sensing applica-tions TMCs act as the host for active materials.[3] The choice and design of the active metal center are focused on the catalytic reaction, but a crucial question concerns the alterations that the TMC supports can undergo during operational use, which may inadvertently alter performance. Therefore, it is important to identify the intrinsic electrochemical activity of TMC supports.

Among TMC supports, the electrochemical stability of a few (Mo$_2$C, WC) have been investigated and shown to be unstable in some potential ranges limiting their use in electrochemical applications.[7,8] Recently, TiC has been used for sensing biomolecules such as dopamine, ascorbic acid, and hydroquinone.[9,10] In addition, TiC based supports have been claimed to be the best catalyst supports for HER, ORR, and CO$_2$ reduction reactions[11,12] conferring remarkably lower overpoten-tial for these reactions.[12,13] Compared to other 2D SACs such as graphene, transition metal chalcogenides, and boron nitride, metal carbides have several advantages such as ease of preparation, cheap and notably, strong metal-support interac-tion facilitating catalytic reactions.[14,15] Despite these advan-tages, the stability of the support in the relevant experimental environments is an important concern and has received little attention hitherto. In this work, we experimentally investigate the inherent electrochemistry of TiC NP and mimicking the general practical usage, off-the-shelf TiC NPs are examined. We find that the TiC NPs undergo irreversible oxidation at positive potentials (> 0.7 V vs saturated calomel electrode (SCE)) and to an extent that is highly dependent on the pH of the solution. Further, we extended our investigation down to a single NP level by conducting nano-impact measurements under the same experimental conditions revealing further information on NP oxidation.[16]

Experimental Section

Chemicals

TiC nanoparticles (35–50 nm average particle diameter) were procured from Sigma Aldrich. Monosodium hydrogen phosphate (NaH$_2$PO$_4$, ≥99.9%), disodium hydrogen phosphate (Na$_2$HPO$_4$, ≥99.9%), sodium hydroxide (NaOH, ≥99.9%), sulfuric acid (H$_2$SO$_4$), were purchased from Sigma-Aldrich, Dorset, UK, and Fisher Chemicals, NH, USA respectively. All solutions were prepared with ultrapure water from Millipore, with a resistivity of 18.2 MΩcm at 298 K.

[a] Dr. P. Nayak, R.-C. Xie, Prof. R. G. Compton
   Department of Chemistry,
   Physical and Theoretical Chemistry Laboratory
   Oxford University, South Parks Road, Oxford OX1 3QZ, UK
   E-mail: richard.compton@chem.ox.ac.uk
[b] Prof. R. G. Palgrave
   Department of Chemistry, University College London
   20 Gordon Street, London, WC1H 0AJ, UK

Electrochemical Apparatus and Method

All electrochemical experiments were performed with a three-electrode system mounted within a Faraday cage. The working electrode was a glassy carbon of diameter 3.0 mm from ALS, Tokyo, Japan. The reference electrode was a saturated calomel electrode (SCE). All the potentials reported in this work were with respect to the SCE unless specified. A graphite rod was used as the counter electrode. All electrochemical measurements were thermostated at $25 \pm 0.5\,°C$. The electrochemical measurements were performed using a computer-controlled Autolab PGSTAT128N potentiostat (Metrohm Autolab, Utrecht, Netherlands) equipped with GPES software.

Before use, the GCE was polished to a mirror-like finish using alumina slurries in a sequence of decreasing sizes: 1.0, 0.3, and 0.05 μm (from Buehler, Lake Bluff, IL), followed by rinsing and sonicating with DI water to remove the slurry residues. The TiC sample was dispersed in ethanol (1 mg/ml) by ultrasonication for 1 hour. Before each electrochemical measurement, the TiC NPs dispersion was ultrasonicated for 5 minutes to maintain homogeneity. A 2 μL aliquot of the suspension (2 μg of solid) was then drop-casted over a previously cleaned GCE. The solvent was left to evaporate at room temperature to yield an electrode surface modified with a 2 μg film of the TiC NPs. The modified electrode is denoted TiC@GCE and the microscope image of the drop-casted electrode is shown in Figure S1 (Supporting Information). Taking the area of the GCE (7.06 mm^2) and the average NP size (35 nm) a 2 μL (1 mg/ml) dispersion (containing NPs of 35–50 nm range) can form ca 1–2 NP layers averaged over a 3 mm diameter GCE assuming close packing and a uniform deposition covering exclusively the entire disc area. However, some unavoidable local NP agglomeration/aggregation is well known[17] to plague the drop-casting method. Significant heterogeneity was observed for the TiC NP deposits microscopically as detailed in the SI with well-separated clumps of accumulated particles evident. The modified electrode was dried in the air before use. Before electrochemical measurements, the electrolyte was purged with N$_2$ (98% purity) to remove dissolved gases. To measure the intrinsic electrochemistry of the TiC NPs, CV measurements were performed over different scan ranges in both anodic and cathodic directions. In the anodic study, the sample was first scanned toward $+1.8\,V$, followed by a reverse sweep toward $-1.8\,V$ and finally returned to 0 V. Conversely in the cathodic study, the sample was scanned toward $-1.8\,V$ initially, then reversed to $+1.8\,V$, and finally to 0 V. Repeated scans were performed depending on any anticipated informative electrochemical events. Retention of the TiC particles on the electrode surface was demonstrated by the reproducibility of results over five separate independent experiments (Figure S2).

Materials Characterization

XRD patterns were recorded using a Nonius Kappa Geometry X-ray Diffractometer: X-ray source Mo anode (max 60 kV, 300 mA), graphite monochromator, Theta angle: $10°-90°$ ($\pm 0.01°$). As observed (Figure S3a), the peaks corresponding to the face-centered cubic structure of TiC are present (JCPDS no-321383). A small peak corresponding to C (002) is also present along with TiC peaks. This can be due to the presence of a trace amount of residual carbon precursor taken during the carbothermal synthesis of TiC. No dominant peak corresponding to TiO$_2$ is observed from the XRD indicates that no substantial amount of bulk crystalline TiO$_2$ is present.

X-ray photoelectron spectroscopy (XPS) was carried out with a two-chamber Thermo K-alpha spectrometer using a monochromated Al Kalpha X-ray source (1486.6 eV) in a constant analyzer energy mode. X-rays were focused on a 400-micron spot at the sample surface, which defined the analysis area. Sample charging was prevented by the use of a dual-beam flood gun. High-resolution core line spectra were recorded at 20 eV pass energy, and survey spectra were recorded at 150 eV pass energy. Electrode samples were mounted by securing with double-sided carbon tape. The powder sample was adhered directly to the tape. The data were analyzed and peak fitting was done using CASA XPS software. The material preparation for XPS measurements is discussed in the Supporting Information. Figure S3b shows the XPS survey spectra and the deconvoluted short scan in the Ti 2p region. XPS is a surface-sensitive technique with the soft X-rays in XPS penetrating only up to a few nm depths. Along with the doublet peaks corresponding to TiC, doublet peaks corresponding to TiO$_2$ were seen. The surface TiC: TiO$_2$ ratio was calculated to be 72:28 in the deconvoluted spectra. Since metal carbides are oxyphilic, we infer that the surface Ti in TiC reacts with atmospheric oxygen to a certain extent.[18]

Nano-impact Experiments

Nano-impact experiments were carried out with a home-built low-noise three-electrode potentiostat system equipped with a low-noise current amplifier (LCA-4K-1G, FEMTO Messtechnik GmbH, Germany) and a homemade thermostat system.[19] The signal was digitized at 100 KS/s via a USB data acquisition device (USB-6003, National Instruments, Texas, USA) filtered digitally by a four-pole Bessel filter to 100 Hz. The potentiostat has been shown to conserve the charge passed during the impact even at short duration impacts.[20] The nanoparticle impact measurements were thermostated at 25 °C in a Faraday cage. A homemade carbon fiber microelectrode of nominally 7 μm diameter and 1 mm length was used as the working electrode.[21] A SCE and a graphite rod were acted as the reference electrode and the counter electrode, respectively. Chronoamperometry was performed using TiC NPs dispersed in 0.5 M H$_2$SO$_4$ (0.5 mg/10 mL corresponding to approximately ~10^{12} TiC NPs/1 mL) at a range of potentials from 0.9 V–1.3 V. The obtained nano-impact spikes were identified, analyzed and individual spike charge was determined using "Signal Counter" software (developed by Dario Omanovic Centre for Marine and Environmental Research, Zagreb, Croatia).[21]

2. Results and Discussion

2.1. Intrinsic Electrochemistry Study

To investigate the intrinsic electrochemistry of TiC NPs, CVs were first performed at a scan rate of 100 mV s^{-1} in 0.1 M phosphate-buffered saline (PBS, pH 7) as the supporting electrolyte. The voltammetric response was measured in both anodic and cathodic initial directions starting at 0 V corresponding to an initial current close to zero (Figure 1 a,b). Three consecutive scans for TiC@GCE (electrode preparation discussed in the Supporting Information) were performed and compared with a bare GCE (Figure S4 ESI). As observed, the first scan in anodic direction resulted in oxidation peaks at ca. 0.69 V (OX1) and 1.30 V (OX2) followed by a tiny, barely discernible reduction peak at $-0.57\,V$. However, no oxidation is observed in subsequent scans (2nd and 3rd). The first scan towards cathodic potentials from 0.0 to $-1.8\,V$ resulted in H$_2$ evolution current at negative threshold potentials of ca. $-1.00\,V$ and similar redox

ChemElectroChem

Articles
doi.org/10.1002/celc.202001498

**Chemistry
Europe**
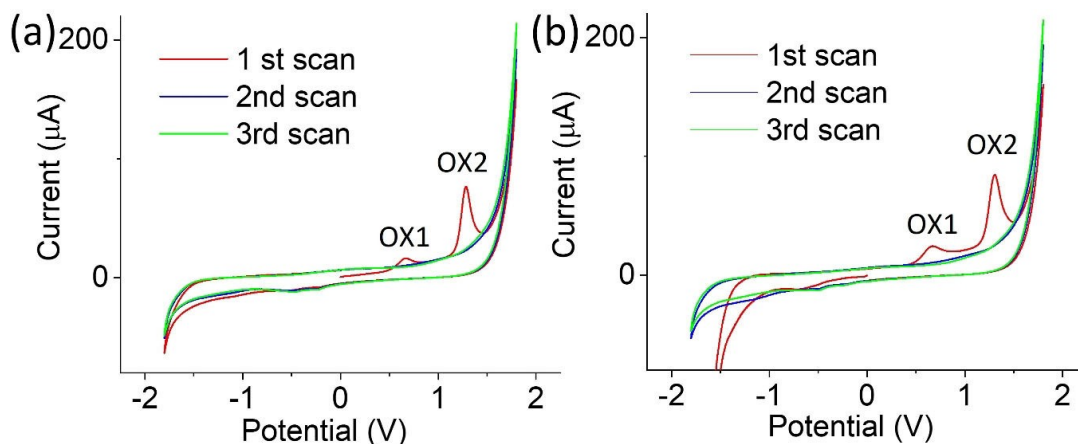European Chemical
Societies Publishing

Figure 1. Cyclic voltammetry for TiC@GCE in a) anodic and b) cathodic directions in 0.1 M PBS, pH 7 for three consecutive cycles (100 mV/s scan rate, SCE as RE).

peaks on the reverse (oxidation) scan. The absence of sustained currents on follow-up scans indicates that the initial oxidation in 1st scan irreversibly passivates the TiC NP surface, which consequently becomes less susceptible to both H_2 evolution and further NP oxidation. No corresponding redox features are observed for a bare GCE (Figure S4, Supporting Information) under the same experimental conditions, indicating the redox behavior observed here stems from TiC NPs. The impact of scanning in different potential ranges, as observed in Figure 2a (i–iv), results in no significant change in redox behavior of TiC under similar experimental conditions. Further, the CVs were recorded for three consecutive scans in PBS of pH 5.8 and 8 in different potential ranges (Figure S5). The observed shift in oxidation peak potential with pH is in general accordance with the Pourbaix diagram of TiC,[22] which we discuss below after

exploring the inherent electrochemistry in acidic medium (low pH).

Having evidenced the intrinsic irreversible oxidation of TiC in PBS, acidic electrolyte (1 M H_2SO_4) was next considered. Figure 2b depicts the CVs collected at a 100 mVs^{-1} scan rate in different potential ranges. Figure 2bi shows CVs from 0 to 1.8 V resulted in OX1 followed by OX2 in the 1st scan, and complete disappearance of these peaks in the follow-up scans. A very similar observation was seen in the 0 to 1.25 V scan range (Figure 2bii), allowing only the OX1 event to occur. These indicate complete passivation of the TiC surface in the 1st scan itself. Next voltammograms were recorded with scans towards negative potentials under the same experimental conditions as shown in Figure 2biii–iv. Scanning over a wide window (−1 to 1.8, Figure 2biv) resulted in OX1 followed by OX2 in the 1st scan. Unlike the redox events in PBS, the subsequent two scans
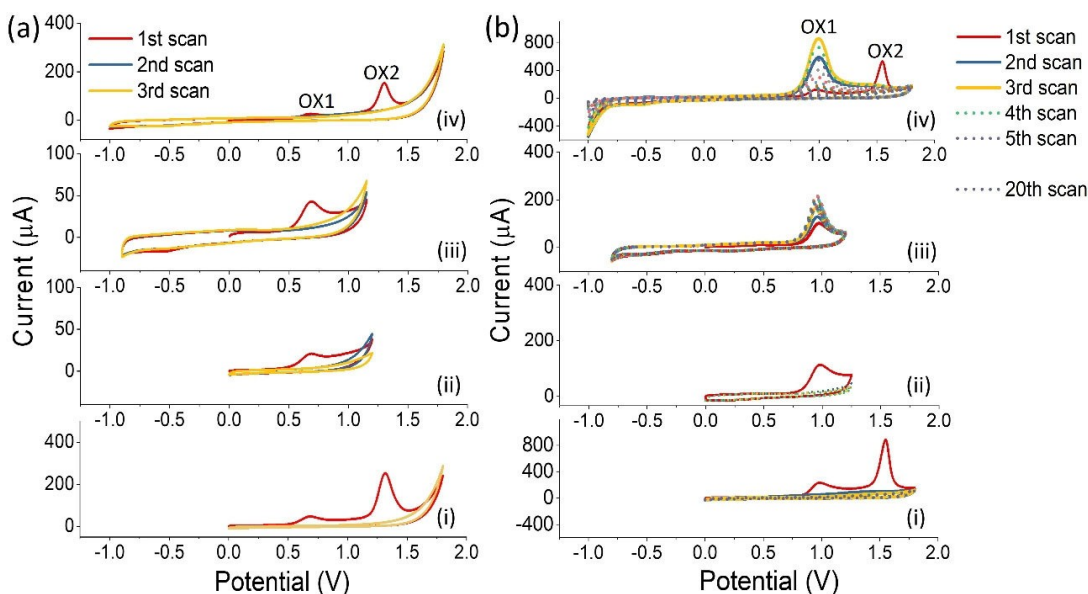

Figure 2. Cyclic voltammetry for TiC@GCE in a) 0.1 M PBS (pH 7) and b) 1 M H_2SO_4 in different scan ranges (100 mV/s scan rate, SCE as RE).

ChemElectroChem

Articles
doi.org/10.1002/celc.202001498

**Chemistry
Europe**
European Chemical
Societies Publishing

increased the OX1 peak current, but a feeble OX2 peak. However, after 3 scans the OX1 peak decreased slowly with complete disappearance after ca. 20 scans. Similarly, scanning in the range from −0.8 to 1.25 V (allowing only OX1) results in an increase of the OX1 peak up to 5 cycles followed by a slow decrease of the OX1 peak even after 20 scans. This suggests a possible reaction in a negative potential window favoring oxidation in repeated cycles.

To reveal the dependence of these redox events on the pH similar voltammetry studies were done in the −1.0 V to 1.8 V range for 0.1 M (pH 1), 0.01 M (pH 1.87), and 1 μM (pH 6) H_2SO_4 (Figure S6a–c, Supporting Information). Redox profiles resembling those seen at pH 0 (Figure 2b) are observed for pH 1, however, no increase in the current of the OX1 peak in repeated scans is observed for higher pHs. The extent of oxidation is strongly dependent on the pH of the acid. This is evident and understood from the disappearance of the OX1 peak at the 20th scan at pH 0, at the 10th scan at pH 1, at the 7th scan at pH 1.87, and the 5th scan at pH 6.
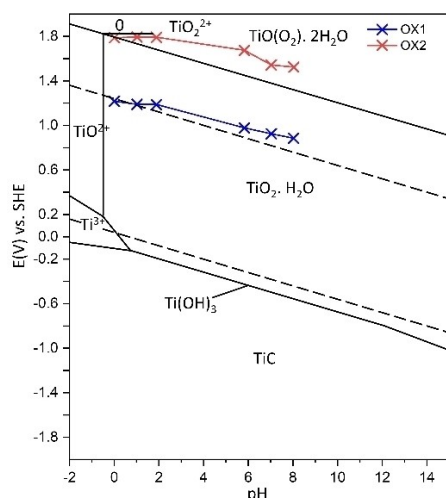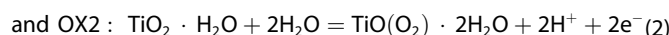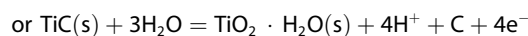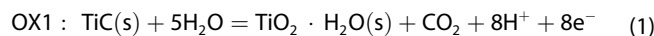

Figure 3. Summary of oxidation peak potentials overlapped on standard Pourbaix diagram of TiC. Adapted from Ref. [22]. Copyright (1972) Elsevier.

Next, the shift of oxidation peak potentials (both OX1 and OX2) are plotted against pH (Figure 3, both PBS and H_2SO_4) and superimposed over the Pourbaix diagram for TiC.[22] As observed, a shift of oxidation peak potential with pH is seen for PBS (pH 5.8-8), which correlates with the data given in the Pourbaix diagram for the phase boundaries between pH 5–8.[22–24]

For TiC, the possible redox events in PBS are [Eqs. (1), (2)]:

$$OX1: \ TiC(s) + 5H_2O = TiO_2 \cdot H_2O(s) + CO_2 + 8H^+ + 8e^- \quad (1)$$

$$or \ TiC(s) + 3H_2O = TiO_2 \cdot H_2O(s) + 4H^+ + C + 4e^-$$

$$and \ OX2: \ TiO_2 \cdot H_2O + 2H_2O = TiO(O_2) \cdot 2H_2O + 2H^+ + 2e^- \quad (2)$$

where $Ti(IV)O(O_2)$ is a peroxy species.[25,26] Besides, there is a strong possibility of C oxidation to CO or CO_2 along with OX2 following Eq. (3) (standard potentials of the C/CO_2 or C/CO redox couples are > 0.9 V vs. RHE in 0.5 M H_2SO_4).[27,28]

$$C + 2H_2O = CO_2(g) + 4H^+ + 4e^-$$

$$Or \ C + 2H_2O = CO(g) + 2H^+ + 2e^- \quad (3)$$
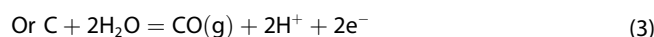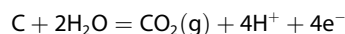
The possible mechanism of oxidation is speculated to be the partial conversion into hydrated TiO_2 ($TiO_2 \cdot H_2O$ in OX1), probably growing inwards from the surface which further oxidizes to $TiO(O_2) \cdot H_2O$ at higher potentials (OX2) along with possible C oxidation as depicted in schematic illustration Figure 4 (i–iv). No redox peak was observed in the repeated scan in PBS indicating that the structural transformation proceeds up to step (iv) in the scheme. Unlike the key observations in PBS, no major shift of oxidation peaks (OX1 and OX2) was observed for the H_2SO_4 medium. The assigned oxidation events according to the Pourbaix diagram are Eq. (1) along with the following Eq. (4):[29]
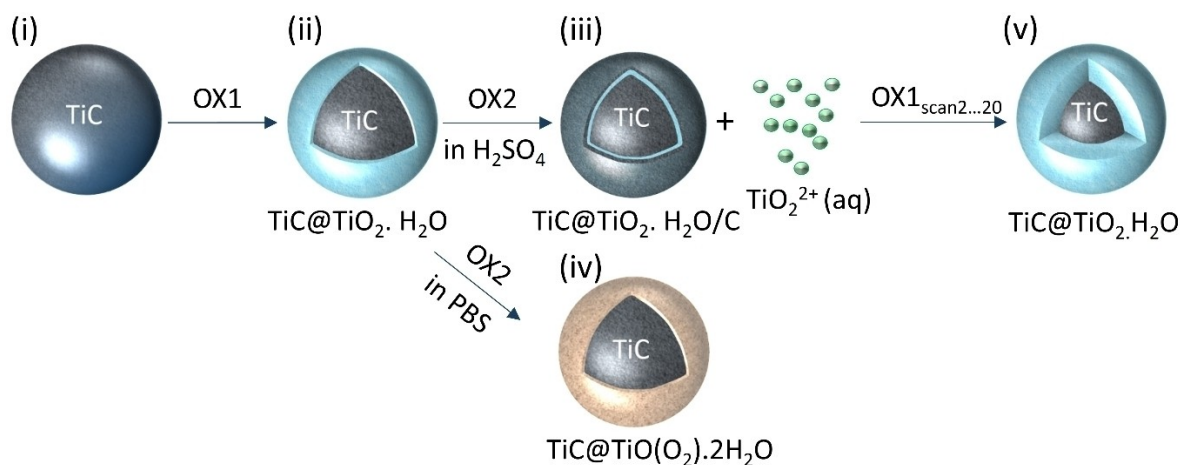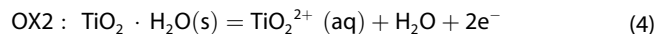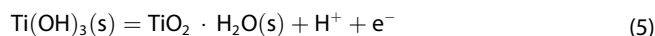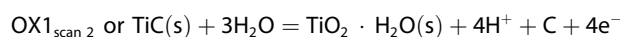
$$OX2: \ TiO_2 \cdot H_2O(s) = TiO_2^{2+}(aq) + H_2O + 2e^- \quad (4)$$

Figure 4. Schematic depiction of the structural alternation of TiC NP during OX1 and OX2 redox events.

ChemElectroChem

Articles
doi.org/10.1002/celc.202001498

Chemistry Europe
European Chemical
Societies Publishing

Again a plausible mechanism is speculated to be the conversion of surface Ti into TiO_2 or hydrated TiO_2 ($TiO_2 \cdot H_2O$ in OX1), which further oxidizes to TiO_2^{2+}(aq) at higher potential (OX2), apparently leaving a possible remnant carbon layer after dissolution (OX2) preventing further oxidation/dissolution in follow-up scans (Figure 2bi).[30] However, scanning towards -1 V may transform Ti(IV) to Ti(III) (in the form of $Ti(OH)_3$) and TiC at extreme negative potentials following the Pourbaix diagram.[29] These features overall indicate the OX1 event in the 2nd scan might be a combination of TiC converting to $TiO_2 \cdot H_2O$ along with the conversion of $Ti(OH)_3$ into $TiO_2 \cdot H_2O$ following the eq 5. Also, comparatively more charge in OX2 may be due to oxidation of carbon at higher potential along with $TiO_2 \cdot H_2O$ dissolution (eq 4).[31,32]

$$TiC(s) + 5H_2O = TiO_2 \cdot H_2O(s) + CO_2 + 8H^+ + 8e^-$$

$$OX1_{scan\ 2}\ or\ TiC(s) + 3H_2O = TiO_2 \cdot H_2O(s) + 4H^+ + C + 4e^-$$

$$Ti(OH)_3(s) = TiO_2 \cdot H_2O(s) + H^+ + e^- \tag{5}$$
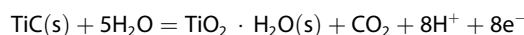
Therefore, it is likely that the net formation of $TiO_2 \cdot H_2O$ at low pH leads to "core-shell" particles ($TiC@TiO_2$) on repeated scans (Figure 4 stage v). The average percentage conversion is evaluated from the total charge passed during the multiple scans, summing the oxidative charges in each scan and assuming an 8 electron transfer reaction [Eq. (1)] (the calculation is shown in the Supporting Information in detail, Figure S7–S9). The variation of absolute charges ($Q_{absolute}$), added-up charges ($Q_{added-up}$), and the corresponding % of total Ti converting to TiO_2 with scan number for a single TiC NP is presented in Figure 5a and Table S1 (Supporting Information). The conversion seen was ca. ~60% in 1 M H_2SO_4 (a sum for a number of 20 scans) leading to "core-shell" particles of ~12.5 nm core radius and ~5 nm shell width (calculations shown in Supporting Information). The evolution of the core radius 'R_c' and shell width 'd' with scan number and H_2SO_4

concentration is depicted in Figure 5b. The decrease in 'R_c' and increase in 'd' with scan number is apparent from Figure 5b. Alternatively, if a 4 electron transfer reaction is assumed as given in eq1, the conversion seen is more than 100% of the Ti into TiO_2; we consider the full or partial 8-electron transfer reaction as more likely and the following calculations are based on this number. However, a combination of both reactions cannot be ruled out as the OX2 peak is much larger than the OX1 peak in all pH conditions. In conclusion, the extent of oxidation is highly dependent on acid concentration and the number of scans.

2.2. Nano-Impact Studies

Having evidenced that the TiC NPs undergo irreversible oxidation in the aqueous medium and positive potential window when oxidized as ensembles on an electrode surface, we extended our investigation to the single-particle level. We conducted nano-impact measurements, which record the electrochemical change that a single NP undergoes during a collision with a potentiostated microelectrode surface.[16,33] The charge appears in the form of current spikes and each spike represents the arrival/collision of NP with the electrode during its Brownian motion resulting in NP oxidation/reduction on collision.[34,35] Nano-impact experiments were conducted for TiC NPs (~10^{12} TiC NPs/1 mL) dispersed in 0.5 M H_2SO_4 at electrode potentials ranging from 0.6 V–1.3 V. No spikes are observed at potentials more negative than 0.8 V, however, potentials positive of 0.9 V resulted in distinguishable current spikes, each associated with the oxidation of the NP on collision with the electrode. Typical current-time traces are shown in Figure 6a. The absence of spikes in the chronoamperogram without NPs (Figure S10, Supporting Information) suggests that the current spikes are due to the collision of NPs with the potentiostated electrode surface. At lower potentials, the current of the oxidative spikes is absent or feeble, whereas the amplitude of
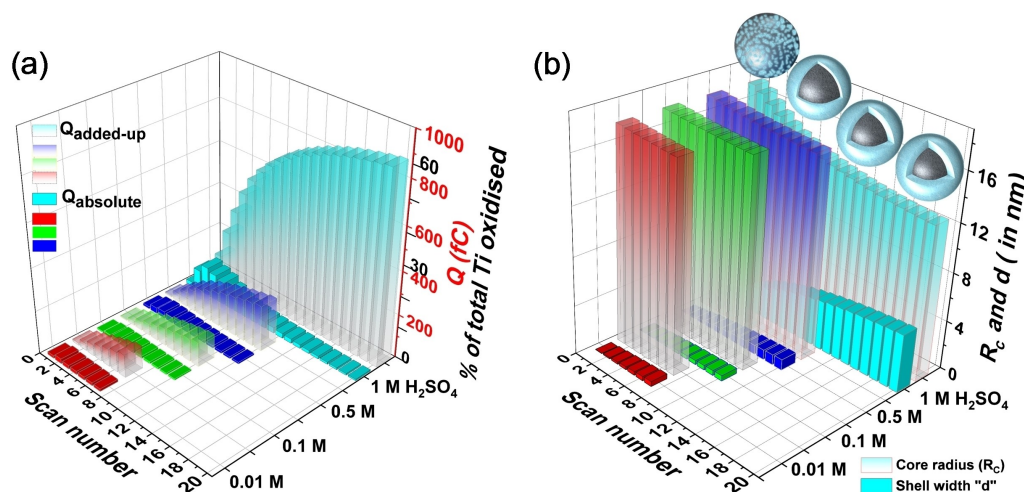

Figure 5. a) Plot of absolute charges ($Q_{absolute}$), added-up charges ($Q_{added-up}$) and % of total Ti converting into TiO_2 vs. scan number for different concentration of H_2SO_4 for a single TiC NP, b) plat of variation of core radius "R_c" and shell width "d" with scan number for different concentrations of H_2SO_4.

ChemElectroChem

Articles
doi.org/10.1002/celc.202001498

**Chemistry
Europe**
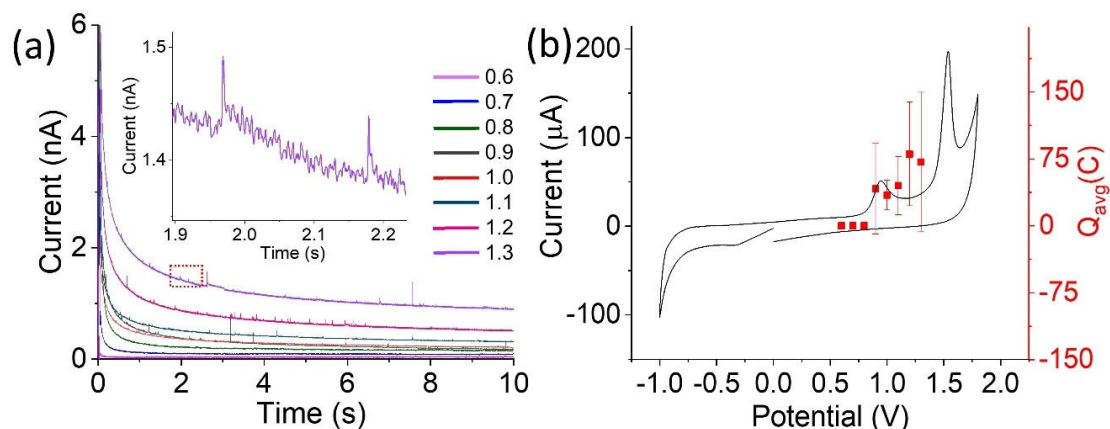
European Chemical
Societies Publishing

Figure 6. a) Chronoamperograms of a carbon fiber micro-wire electrode ($d = 7\ \mu m$) immersed in a 0.5 M H_2SO_4 solution containing 0.1 mg/mL TiC NPs, held at potentials ranging from 0.6 V to 1.3 V vs. SCE. Current spikes are seen as enlarged in insets of (a). b) Overlay of the plot of average impact charge $Q_{(avg)}$ as a function of applied potentials with the voltammogram of TiC NP ensembles immobilized on a GC electrode (100 mV/s scan rate, SCE as RE).

the spikes increases significantly as the applied potential becomes more positive (ca. 1.3 V), consistent with greater NP oxidation at higher potentials.

2.3. Comparison of Nano-Impact and CV Data

The average charge transferred (Q_{avg}) on the impacts of NPs at various potentials is plotted and overlaid with CV in Figure 6b. As observed, the threshold potential for oxidation is 0.9 V, which correlates with the peak in the CV as shown in Figure 6b. At the highest potential (1.3 V), Q_{avg} is calculated to be ~ 72 fC, which is high compared to the charge per NP from the CV of drop-casted electrodes ($Q_{avg} \approx 11$ fC, calculated from the first scan). The average duration of the current spikes is ~ 5 milliseconds which corresponds to a shorter duration than required for the voltammetric scans. A plausible explanation for the discrepancy in the charges passed between the impact and CV experiments may relate to the difficulty of charge propagation between the NPs on the drop-casted electrode (Figure S1) notably within the clumps of aggregated nano-particles. As discussed in the experimental section, the drop-cast NPs undergo unavoidable partial aggregation (seen in the microscope image shown in the Supporting Information), which leads to their incomplete participation in the oxidation event. As such, the nano-impact data is thought to give a more reliable indication of oxidation of $\sim 5\%$ of total Ti in TiC NPs which shows a maximum under 1.3 V applied potential and 0.5 M H_2SO_4 conditions corresponding to an average core-shell structure of a ~ 12.5 nm radius core and a shell of thickness ca ~ 0.5 nm, equivalent to ~ 1–2 layers of surface TiO_2.

2.4. Surface Characterization of the Electro-Oxidation Chemistry

To further confirm and support the formation of TiO_2 over TiC NPs during electro-oxidation, XPS was carried out for TiC NPs

before and after the oxidation event (Figure S3b and S11). The details of electrode preparation for XPS measurement are discussed in the ESI. Note that no TiO_2 peaks were observed in the XRD spectra of TiC NPs (Figure S3a) consistent with the absence of bulk crystalline TiO_2. However, some TiO_2 was detected by XPS (surface TiC: TiO_2 ratio $= 72:28$) in TiC NPs attributed to their oxyphilic nature.[18] After oxidation, the percentage of TiO_2 increased substantially (Figure S1) compared to TiC before oxidation (Figure S3b). This confirms that the electro-oxidation leads to the partial conversion of TiC NPs into TiO_2 validating our claims based on the reported voltammetry.

3. Conclusions

We have investigated the intrinsic electrochemistry of TiC NPs in detail. These are shown to be electroactive in aqueous solution in the pH range 0 to 8 as evident from the two redox signals in a positive potential window and assigned to surface oxidation of Ti into $TiO_2 \cdot H_2O$, dissolution of $TiO_2 \cdot H_2O$ into TiO_2^{2+} (in acids), and transformation of $TiO_2 \cdot H_2O$ into $TiO(O_2) \cdot 2H_2O$ (in PBS). The processes are found to be highly dependent on the pH of the electrolyte medium. Up to ca. 60% of Ti in TiC NPs is oxidized under highly acidic conditions (1 M H_2SO_4) in a total of 20 successive scans leading to "core-shell" particles of ~ 12.5 nm core radius and ~ 5 nm shell width. Further investigations on the surface oxidation of the NPs at a single NP level (nano-impact) revealed a ~ 72 fC charge equivalent to the oxidation of ~ 1–2 layers of surface Ti in TiC NP. This shows very good consistency with the CV results, validating the intrinsic oxidation of TiC NPs. Therefore, the present investigation concludes the surface oxidation of TiC NPs forming TiC@TiO_2 core-shell structures at positive potentials in an aqueous medium.

ChemElectroChem

Articles
doi.org/10.1002/celc.202001498

Chemistry Europe
European Chemical
Societies Publishing

Conflict of Interest

The authors declare no conflict of interest.

[1] Y. Liu, T. G. Kelly, J. G. Chen, W. E. Mustain, *ACS Catal.* **2013**, *3*, 1184–1194.
[2] S. Yang, Y. J. Tak, J. Kim, A. Soon, H. Lee, *ACS Catal.* **2017**, *7*, 1301–1307.
[3] T. Maiyalagan, P. Kannan, M. J-Niedziolka, J. N-Jönsson, *Anal. Chem.* **2014**, *86*, 7849–7857.
[4] S. Shin, J. Kim, S. Park, H.-E. Kim, Y.-E. Sung, H. Lee, *Chem. Commun.* **2019**, *55*, 6389.
[5] D. V. Esposito, S. T. Hunt, Y. C. Kimmel, J. G. Chen, *J. Am. Chem. Soc.* **2012**, *134*, 3025–3033.
[6] S. Saha, B. Martin, B. Leonard, D. Li, *J. Mater. Chem. A* **2016**, *4*, 9253.
[7] M. C. Weidman, D. V. Esposito, I. J. Hsu, J. G. Chen, *J. Electrochem. Soc.* **2010**, *157*, 179–188.
[8] M. C. Weidman, D. V. Esposito, Y.-C. Hsu, J. G. Chen, *J. Power Sources* **2012**, *202*, 11–17.
[9] S. J. Stott, R. J. Mortimer, S. E. Dann, M. Oyama, F. Marken, *Phys. Chem. Chem. Phys.* **2006**, *8*, 5437–5443.
[10] Q. Guo, T. Wu, L. Liu, H. Hou, S. Chen, L. Wang, *J. Mater. Chem. B* **2018**, *6*, 4610.
[11] S. K. Sahoo, Y. Ye, S. Lee, J. Park, H. Lee, J. Lee, J. W. Han, *ACS Energy Lett.* **2019**, *4*, 126–132.
[12] S. Back, Y. Jung, *ACS Energy Lett.* **2017**, *2*, 969–975.
[13] X. D. Lin, Y. G. Zhou, *J. Phys. Condens. Matter* **2019**, *31*, 355302.
[14] R. Gusmão, M. Veselý, Z. Sofer, *ACS Catal.* **2020**, *10*, 9634–9648.
[15] Z. Li, L. Yu, C. Milligan, T. Ma, L. Zhou, Y. Cui, Z. Qi, N. Libretto, B. Xu, J. Luo, E. Shi, Z. Wu, H. Xin, W. N. Delgass, J. T. Miller, Y. Wu, *Nat. Commun.* **2018**, *9*, 5258.
[16] S. V. Sokolov, S. Eloul, E. Katelhon, C. Batchelor-McAuley, R. G. Compton, *Phys. Chem. Chem. Phys.* **2017**, *19*, 28.
[17] Y. Zhang, A. K. S. Kumar, D. Li, M. Yang, R. G. Compton, *ChemElectroChem* **2020**, *7*, 4614–4624.
[18] Z. Li, L. Yu, C. Milligan, T. Ma, L. Zhou, Y. Cui, Z. Qi, N. Libretto, B. Xu, J. Luo, E. Shi, Z. Wu, H. Xin, W. N. Delgass, J. T. Miller, Y. Wu, *Nat. Commun.* **2018**, *9*, 5258.
[19] C. Batchelor-McAuley, J. Ellison, K. Tschulik, P. L. Hurst, R. Boldt, R. G. Compton, *Analyst* **2015**, *140*, 5048–5054.
[20] J. Ellison, C. Batchelor-McAuley, K. Tschulik, R. G. Compton, *Sens. Actuators B* **2014**, *200*, 47–52.
[21] J. Ellison, K. Tschulik, E. J. Stuart, K. Jurkschat, D. Omanovic, M. Uhlemann, A. Crossley, R. G. Compton, *ChemistryOpen.* **2013**, *2*, 69–75.
[22] H. E. Hintermann, A. C. Riddiford, R. D. Cowling, J. Malyszko, *Electrodeposition Surf. Treat.* **1972**, *73*, 59.
[23] A. D. Batter, J.-O. Carlsson, *J. Phys. IV* **1991**, *I*, 641–648.
[24] R. D. Cowling, H. E. Hintermann, *J. Electrochem. Soc.* **1970**, *117*, 1447.
[25] J. Muhleback, K. Muller, G. Schwarzenbach, *Inorg. Chem.* **1970**, *9*, 2381–2390.
[26] D. Schwarzenbach, *Inorg. Chem.* **1970**, *9*, 2391–2397.
[27] J. Willsau, J. Heitbaum, *J. Electroanal. Chem.* **1984**, *161*, 93–101.
[28] S. Möller, S. Barwe, J. Masa, D. Wintrich, S. Seisel, H. Baltruschat, W. Schuhmann, *Angew. Chem. Int. Ed.* **2020**, *59*, 1585–1589.
[29] C. M. Alloca, W. S. Williams, A. E. Kaloyeros, *J. Electrochem. Soc.* **1987**, *134*, 3170.
[30] M. Messner, D. J. Walczyk, B. G. Palazzo, Z. A. Norris, G. Taylor, J. Carroll, T. X. Pham, J. D. Hettinger, L. Yu, *J. Electrochem. Soc.* **2018**, *165*, 3107–3114.
[31] N. Heide, B. Siemensmeyer, J. W. Schultze, *Surf. Interface Anal.* **1992**, *19*, 423–429.
[32] S. Perez-Rodríguez, E. Pastor, M. J. Lazaro, *Int. J. Hydrogen Energy* **2018**, *43*, 7911–7922.
[33] R. Xie, C. Batchelor-McAuley, N. P. Young, R. G. Compton, *Nanoscale* **2019**, *11*, 1720.
[34] E. J. F. Dickinson, N. V. Rees, R. G. Compton, *Chem. Phys. Lett.* **2012**, *528*, 44–48.
[35] M. Ivanovskaya, E. Ovodok, D. Kotsikau, I. Azarko, M. Micusik, M. Omastova, V. Golovanov, *RSC Adv.* **2020**, *10*, 25602–25608.
[36] P. Nayak, N. Kurra, C. Xia, H. N. Alshareef, *Adv. Electron. Mater.* **2016**, *2*, 1600185.